Canadian Geotechnical Journal

OPEN ACCESS | Article

Measurement of pile uplift forces due to soil heave in expansive clays

T.S. da Silva Burke[a], **S.W. Jacobsz**[a], **M.Z.E.B. Elshafie**[b], **and A.S. Osman**[c]

[a]Department of Civil Engineering, University of Pretoria, Pretoria, South Africa; [b]Department of Civil & Architectural Engineering, College of Engineering, Qatar University, Doha, Qatar; [c]Department of Engineering, Durham University, Durham, United Kingdom

Corresponding author: **T.S. da Silva Burke** (email: talia.burke@up.ac.za)

Abstract

Piled foundations are widely used to limit the movement of foundations in expansive clays. These piles are subjected to large uplift forces as the clay swells (and downdrag forces when it shrinks). The appropriate method to estimate these forces is not well understood, and estimates from various methods presented in literature result in large variations. The uplift force generated in piles by soil heave was derived from strain measurements in full-scale field tests where a pile was installed in a highly expansive soil profile and flooded for several months. The results were compared to available theoretical estimates to comment on the most appropriate procedure to estimate the generated tension in the pile. The results showed that the use of an elastic solution related to the expected soil heave combined with a limiting shaft friction estimated from total stress capacity methods provided the most appropriate match to the measured results both in terms of the magnitude of the developed tension in the pile and shape of the tension profile along the depth of the pile.

Key words: piled foundations, expansive clay, field testing

Résumé

Les fondations sur pieux sont largement utilisées pour limiter le mouvement des fondations dans les argiles expansives. Ces pieux sont soumis à d'importantes forces de soulèvement lorsque l'argile gonfle (et à des forces de retrait lorsqu'elle se rétracte). La méthode appropriée pour estimer ces forces n'est pas bien comprise, et les estimations obtenues à partir de diverses méthodes présentées dans la littérature donnent lieu à de grandes variations. La force de soulèvement générée dans les pieux par le soulèvement du sol a été calculée à partir des mesures de déformation effectuées lors d'essais en grandeur réelle sur le terrain, où un pieu a été installé dans un profil de sol très expansif et inondé pendant plusieurs mois. Les résultats ont été comparés aux estimations théoriques disponibles afin de commenter la procédure la plus appropriée pour estimer la tension générée dans le pieu. Les résultats ont montré que l'utilisation d'une solution élastique liée au soulèvement du sol prévu, combinée à un frottement limite de l'arbre estimé à partir des méthodes de capacité de contrainte totale, a fourni la correspondance la plus appropriée aux résultats mesurés, à la fois en termes d'ampleur de la tension développée dans le pieu et de forme du profil de tension le long de la profondeur du pieu. [Traduit par la Rédaction]

Mots-clés : fondations sur pieux, argile expansive, essais sur le terrain

1. Introduction

Expansive clays, also known as swelling clays, are clays that undergo a large volume change as a result of a change in moisture content. They predominantly consist of clay minerals of the smectite group. During wet periods, as the water content of the soil increases, the clay expands causing surface heave (upward vertical movement); during dry periods, the soil dries out and shrinks, and large surface cracks are often visible. This cyclical change in volume causes significant potential for distress to roads and infrastructure founded in these areas. Large cracks often appear as a result of differential movement if the foundations are not adequately designed to resist this movement.

Expansive clays are located in arid and semi-arid regions around the world; notable deposits are located in Sudan, South Sudan, Tanzania, India, and Australia (Morin 1971). South Africa and Texas, USA are also known to have problems associated with expansive clays (Jones and Holtz 1973; Williams et al. 1985).

Piled foundations are widely used to limit the movement of foundations in expansive clays. The piles are socketed below the active zone where moisture changes and thus volume changes are negligible, preferably in a stable nonexpansive layer to reduce uplift of the structure; this is shown in Fig. 1. The expansive clay in the active zone swells, thus applying an uplift force to the pile. This is resisted by the length of the

Fig. 1. Problem definition of piles in expansive soils.

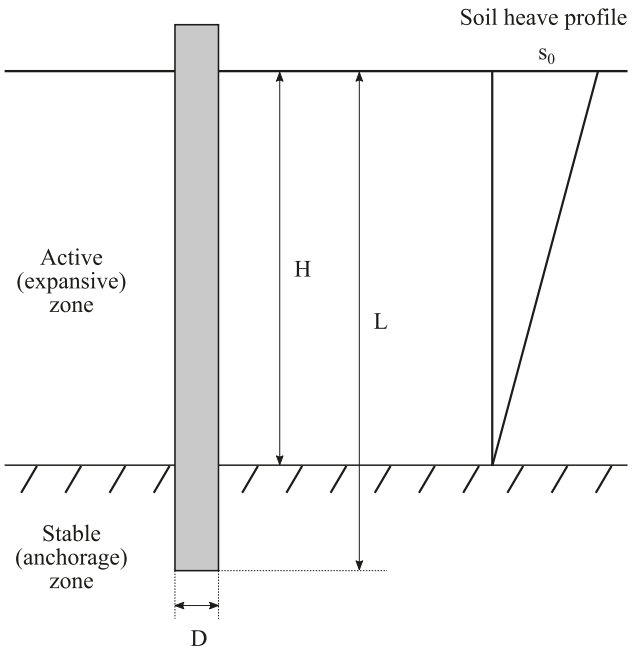

pile in the anchorage zone. To appropriately design the piles, the expected heave forces applied by the expansive clay on the pile shaft need to be understood.

Limited experimental data on the uplift force generated in long piles by expansive clays are available to check against theoretical relationships; where this does exist, this is usually the result of laboratory or centrifuge studies, for example Challa and Poulos (1991) and Fan et al. (2007), or a back-analysis of working piles where uplift has been recorded, for example Collins (1953) and Meintjes and Pellissier (1994). This study was therefore undertaken to provide detailed experimental measurements of the uplift force generated in piles by soil heave in full-scale field tests, and compare this to available theoretical estimates to comment on the most appropriate procedure to estimate the generated tension in the pile.

2. Background

Several procedures exist to estimate the uplift force generated on a pile due to soil heave; these can be grouped into total stress, frictional or effective stress, and elasticity methods, and are outlined below.

2.1. Total stress methods

Total stress methods use the undrained shear strength to directly estimate the shaft friction. The uplift force is calculated using the average pile–soil adhesion over the surface area of the pile (eq. 1) where α is the pile shaft adhesion factor, c_u is the undrained shear strength of the soil, D is the pile diameter, and H is the depth of the active layer; this has also been called the α method following the total stress method used by Skempton (1959). The recommended value of α is 0.45 (Elsharief et al. 2016; Byrne et al. 2019);

$$F_u = \alpha c_u \pi D H \quad (1)$$

2.2. Frictional methods

Frictional or effective stress methods to estimate uplift forces consider the shaft friction generated by movement of the soil against the shaft. This has also been called the β method (Chandler 1968; Burland 1973). Collins (1953) assumed that tensile forces are developed in the pile due to the shaft friction between the soil and the pile. For rough bored piles, the slip surface occurs in the soil, and the shear strength between the soil and the pile can be assumed to equal the shear strength of the soil. For sufficient movement, the full shear strength is mobilised (assuming full slip, use residual shear strength values), and the shaft friction, f, is given by

$$f = c' + \sigma_h' \tan\phi' \quad (2)$$
$$\sigma_h' = K\sigma_v' = K\gamma h$$

where c' is the cohesion intercept, ϕ' is the effective internal angle of friction, γ is the unit weight of the soil assuming a deep water table, and h is the depth from the soil surface. K is the coefficient of lateral stress. Collins (1953) highlighted that K varies from 0.5 to 2.0, but the expected long-term value is expected to be 1.0. Poulos and Davis (1980) recommended that for a soil swelling from an initially unsaturated state, the use of total instead of effective overburden stress in eq. 2 is recommended.

The total uplift force, F_u, is calculated as the integral of the shaft friction from the soil surface to the bottom of the active layer. For constant pile diameter and soil properties, this is calculated as

$$F_u = 0.5\pi D\left(2c'H + K\gamma H^2 \tan\phi'\right) \quad (3)$$

where D is the pile diameter and H is the depth of the active clay layer.

Blight (1984) also used this method to evaluate the shaft friction due to heave which could then be used to calculate the tensile force in the pile. Their tests showed an increase in shaft friction in wet tests compared to that induced under natural moisture content (NMC). This was attributed to increased lateral stress in the wet soil due to swelling pressure from the clay. To account for this, their recommendation was to use $K = 1$ for saturated conditions and $K = 0.5$ for soils at NMC.

2.3. Elastic solution

Poulos and Davis (1980) describe an approach to solve for the tension developed in a pile in a swelling clay using an elastic method which calculates the tension in the pile by applying a specified movement of the soil as induced by soil heaving. A numerical analysis or the use of developed software (for example, Poulos 1989) is required to solve for the tension in the pile.

Xiao et al. (2011) and Fan et al. (2007) developed an elastic method that uses the movement of the soil against the pile to determine the axial force, P, in the pile as a function of the depth, z. The solution is shown in eq. 4 and has been developed with the sign convention that upward movement of the

soil or pile is negative, and tension in the pile is negative. A linear heave profile with depth from the surface to the depth of the active zone is assumed in the free-field soil, as shown in Fig. 1. The soil movement against the pile is then determined using the shear deformation of the soil. This solution was validated against model testing reported by Fan et al. (2007), and showed similar results to the elastic method of Poulos and Davis (1980). An update to this method is presented by Jiang et al. (2020) who consider the linear variation of the shear modulus of soil, G_s, with depth (as opposed to the constant modulus used by Xiao et al. (2011) and Fan et al. (2007)). This had the effect of lowering the location of the maximum tensile force induced in the pile, but did not significantly affect the magnitude of this maximum; for the sake of simplicity, the formulation with constant shear modulus is used in this analysis;

$$P(z) = \begin{cases} -E_p A_p \left(\alpha C_1 \cosh(\alpha z) + \alpha C_2 \sinh(\alpha z) + s_0/H\right); \\ \quad 0 \le z \le H \\ -E_p A_p \left(\alpha C_3 \cosh(\alpha z) + \alpha C_4 \sinh(\alpha z)\right); \\ \quad H \le z \le L \end{cases} \tag{4}$$

where E_p is the modulus of elasticity of the pile, A_p is the pile cross-sectional area, $\alpha^2 = 2\pi/\lambda_p A_p \zeta$ [$\zeta = \ln(r_m/r_0)$; $r_m = 2.5L(1-\nu)$; $\lambda_p = E_p/G_s$], s_0 is the magnitude of the surface heave, and the coefficients are calculated as

$$C_1 = -\frac{s_0}{\alpha H}$$

$$C_2 = C_4 + \frac{s_0}{\alpha H}\sinh(\alpha H)$$

$$C_3 = C_1 + \frac{s_0}{\alpha H}\cosh(\alpha H)$$

$$C_4 = -\frac{\cosh(\alpha L)}{\sinh(\alpha L)}C_3$$

The coefficients presented by Xiao et al. (2011) for use in eq. 4 are not the same as those presented by Fan et al. (2007); neither of the sets of coefficients in either paper results in the ability to reproduce their own results in the figures and parametric studies in these papers. It is expected that there are unintended errors in the reproduction of the coefficients in both papers. The coefficients presented above have been recalculated; full details of the derivation are provided in the supplementary information.

The benefit of this elastic method is that it provides a closed-form solution, and is able to provide a simple prediction with a direct relation to the in-situ soil profile and properties of the expansive clay and the ability to provide a correlation between the amount of heave and the tensile force in the pile as would be expected in practice. Methods to determine a predicted value for heave at the soil surface include those of Van der Merwe (1964) and Jennings (1962).

3. Field tests

Full-scale field tests were conducted by installing an instrumented bored concrete pile in an expansive soil layer and measuring the strain generated in the pile over time. Two piles were installed: one was kept at natural moisture content (NMC), and the other was surrounded by a berm with infiltration wells in the clay and flooded to induce swelling in the clay. The piles were drilled through the depth of the expansive soil layer, and anchored in the soft rock stratum below. The site characterisation, pile instrumentation and field installation are detailed below.

Fig. 2. Expansive potential of the clays on site plotted according to the activity chart of Van der Merwe (1964). [Colour online]

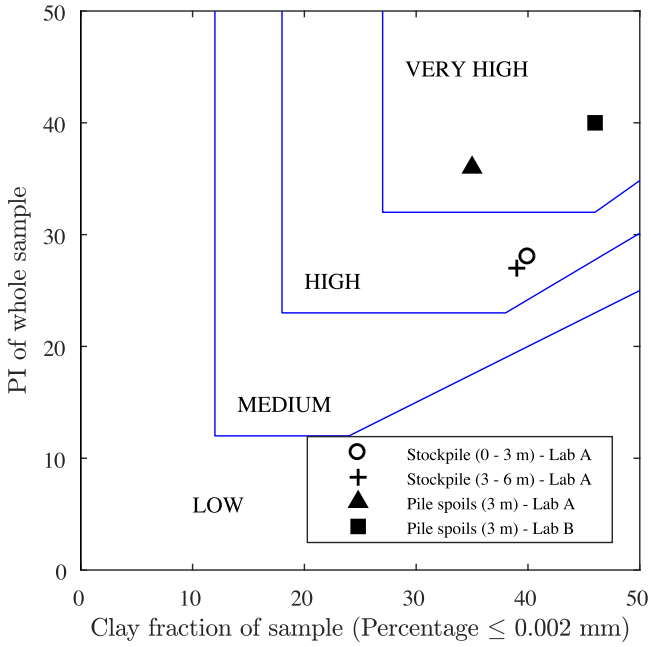

3.1. Site location and characterisation

The field tests were conducted on the site of an existing clay quarry in the Free State province of South Africa between the towns of Kroonstad and Vredefort. Clays are excavated on site by shallow surface mining to a depth of approximately 6 m and stockpiled for further processing. This site was selected due to the large open area, presence of a known, thick expansive clay (⩾6 m) from the surface and absence of nearby infrastructure likely to be impacted by the testing.

The site is located in an alluvial plain underlain by lavas of the Klipriviersberg Group; this group consists of basic igneous rocks (basalt and andesite). The transported and residual soil layers in this region are predominantly clayey. The expansive nature of the soil is likely due to a combination of active material transported from the weathering of the adjacent basic igneous rocks as well as the in situ weathering of the underlying basic rocks.

Samples of clay were taken from the stockpiles of excavated material on site and sent for preliminary grading and indicator tests. These stockpiles had been created from material excavated several years earlier, and were thus only able to give a general indication of soil classification as a result of potential changes due to weathering and exposure. Figure 2

Fig. 3. Simplified borehole logs with the expansive material highlighted. [Colour online]

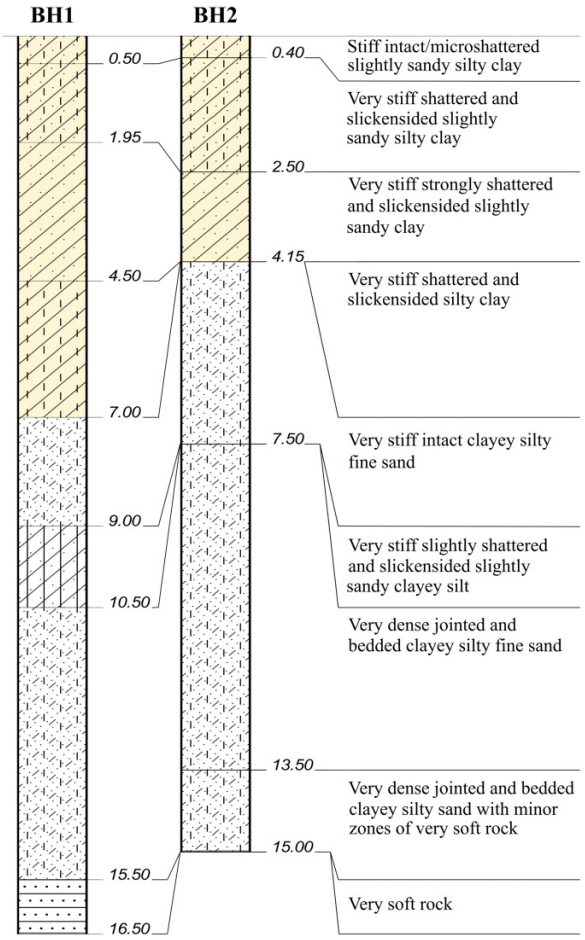

presents the activity chart as per Van der Merwe (1964), indicating potential expansiveness based on the plasticity index (PI) of the whole sample and clay fraction; both samples fall within the high expansive region. These results confirmed the suitability of the material on site for the intended field-testing.

Two rotary core boreholes were drilled in the vicinity of the intended pile installation area to confirm the soil profile and determine the depth to the underlying rock strata. The simplified soil profile is shown in Fig. 3. The extent of the shattered and slickensided alluvial material gives an indication of a 7 m thick expansive layer in BH1, reducing to ≈4 m in BH2. This was underlain by presumed residual material. A very soft rock was encountered at 15.5 m in BH1; BH2 was stopped at 15 m depth where minor zones of soft rock were encountered. There was no free water in the boreholes; an attempt was made to take undisturbed samples; however, the soil was too stiff to allow penetration of the sample tubes.

Samples of soil from within the SPT sampler were collected from BH1, and the suction was measured using a WP4C Dewpoint Hygrometer. There is likely some change from the true in situ condition due to disturbance and fluid from the drilling process; the collection of samples from the core of the SPT sample aimed to minimise this. Suctions of 1 and 0.43 MPa were measured at depths of 1.95 and 6.45 m. No suction was measured in samples taken below 6.45 m; this shows a change from negative to positive soil water pressure at a depth approximately coinciding with the transition from an expansive transported clay to residual sand.

The completion of the initial site characterisation showed an expansive layer thick enough to generate measurable uplift forces in a pile installed in this profile, plus an inactive area below and soft rock that would act as a socket preventing free movement of the pile. Further detail of field test design is described in the following section.

3.2. Pile instrumentation

Two instrumented piles were installed for the investigation of tension developed in bored concrete piles due to soil heave. The test piles were located in a large flat area that was free of large vegetation that would significantly influence the soil moisture regime. One pile was kept at natural moisture conditions as a control, i.e., the “Dry Pile”. A berm was constructed around the second pile, and this area was flooded to induce accelerated heave of the expansive soil. This pile was called the “Wet Pile”, and was located in the area with a thicker expansive soil profile to the east of the site near to where BH1 was drilled as the thicker expansive clay would generate larger tensile forces in the pile. Stone-filled infiltration wells with a depth of 6 m and diameter of 100 mm were installed within the berm area to facilitate quicker and more complete saturation of the expansive clay layer.

The dry pile was located a minimum of 50 m away from the boundary of the wet test area to be beyond the presumed radius of influence of the flooded area. An array of soil surface monitoring points was installed around the piles to monitor the change in soil surface level over time; the array is set up to include monitoring of other piles not reported in this paper.

A schematic representation of the pile design and instrumentation showing the idealised soil profile for each pile is presented in Fig. 4. The pile diameter was 450 mm; a thinner pile than would conventionally be installed for a deep foundation was chosen to generate a more extreme tensile response through the depth of the pile. The total length of the pile was 16.5 m; using preliminary predictions of the expected tensile force generated by the expansive soil, the anchorage provided by the residual sandy layers and a 1 m socket in the very soft rock was sufficient to prevent free movement of the pile.

The piles were instrumented with pairs of vibrating wire strain gauges (VWSGs) at six levels (12 gauges total per pile); these levels were 1, 3, 5, 7 and 9 m from the top, and 2 m from bottom (14.5 m from the top). The gauges used were Geosense VWS 2100 embedment gauges. A higher instrumentation density was provided in the region in the expansive clay as this is where the greatest rate of change in pile tension was expected. The gauges were mounted in-between two longitudinal reinforcement bars using short bars placed across the longitudinal bar to maintain the position and verticality of the VWSG.

Fig. 4. Schematic representation of the pile instrumentation showing idealised soil profile (vertical scale 4× horizontal scale). [Colour online]

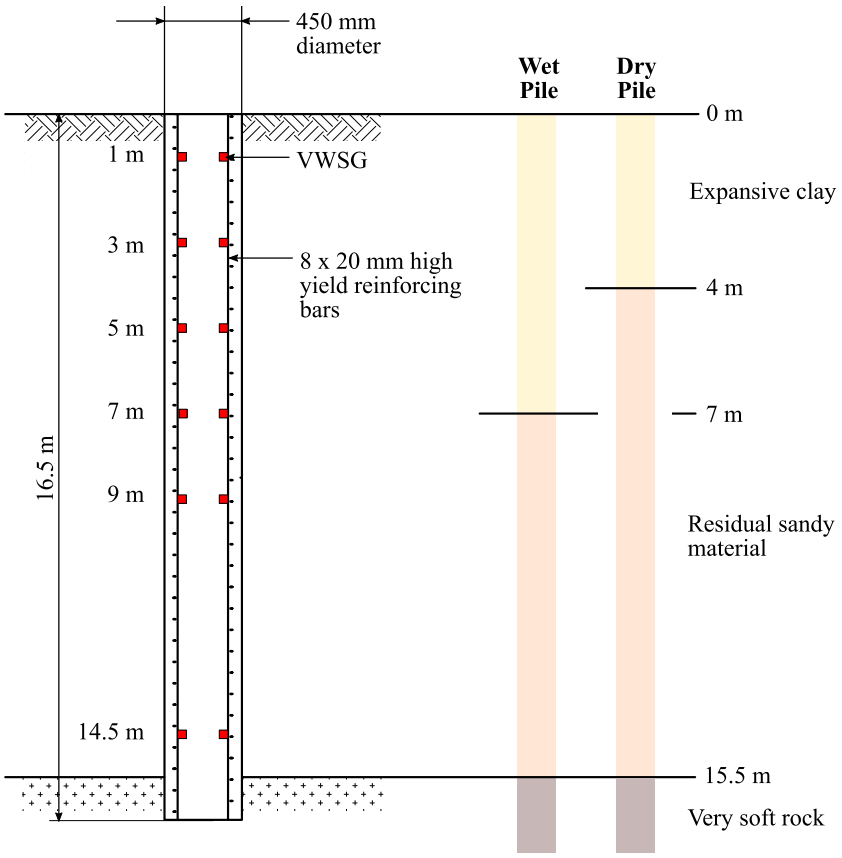

3.3. Field installation

The piles were cast on 29 and 30 January 2020 (wet and dry pile respectively); this was towards the end of the wet season when the soil would be expected to be at its maximum natural heave in an annual cycle. The installation was conducted after a period of heavy rainfall on site.

One month after the pile installation had been completed, i.e. once concrete could be presumed to be at full strength, the area within the berms around the wet pile was flooded and data logging of the instruments was started. The wet pile area was kept flooded for six months (up until the end of September 2020) with periodic checks to top up the water level by pumping from the nearby quarry. Thereafter, the surface was allowed to naturally dry out. Monitoring was continued for a further five months.

3.4. Soil and concrete properties

A soil sample obtained from the bored pile drilling spoils at 3 m depth for the wet pile was taken to confirm the expansive potential characterisation and determine the soil properties needed for further analysis and investigation. The fresh material showed higher expansive potential than the stockpiled material and classified as having very high expansive potential (see Fig. 2). The soil grading and indicator properties are shown in Table 1. The soil sample was sent to two laboratories for independent confirmation of the results; despite wide variance in the clay fraction, the overall characterisation of the soil was consistent.

The in situ moisture content was measured from samples taken from the auger spoils at 1 m intervals up to a depth of 6 m; the corresponding bulk density was calculated on material clods using the wax density method, and the resultant void ratio and degree of saturation were calculated. The specific gravity of this material was determined using a pycnometer. The results of these characterisations are shown in Table 2. A series of consolidated undrained triaxial tests were conducted at effective stresses of 100, 200, and 300 kPa to establish the effective stress parameters of the soil; these results are also included in Table 2

The drying soil water retention curve (SWRC) and the shrinkage curve (SC) of the upper clay profile were measured on samples 15 mm in diameter and 10 mm in height in the WP4C. Saturated samples were prepared to a target dry density of 1450 kg/m^3 (average in situ value); the small sample size was chosen to limit the impact of shrinkage cracks on volume measurements. The results are shown in Fig. 5. The best-fit curves according to the forms suggested by Fredlund and Xing (1994) and Fredlund et al. (2002) for the SWRC and SC respectively are shown in the figures. The in situ condition is shown on the shrinkage curve; the measured soil suctions on site were lower than 1 MPa, and thus do not plot on the scale of the shown SWRC. The shrinkage curve plot shows

Table 1. Grading and indicator properties of soil characterised from borehole drilling spoils.

Soil property	Unit	Lab A*	Lab B†
Gravel	%	3.2	0
Sand	%	28.2	26
Silt	%	33.6	20
Clay	%	35	54
Liquid limit (LL)	%	76	82
Plastic limit (PL)	%	39	42
Plasticity index (PI)	—	37	40
Linear shrinkage	%	14.5	23.5

*Classifications according to ASTM D422-63e2 (2007).
†Classifications according to SANS 3001-GR1 (2013), SANS 3001-GR3 (2014), and SANS 3001-GR10 (2014).

Table 2. Soil properties.

Soil property	Symbol	Unit	Mean	CV (%)
Specific gravity	G_s	g/cm^3	2.66	—
Moisture content	—	%	21.5	15.4
Bulk density	γ	kg/m^3	1762	3.1
Void ratio	e	%	0.84	10.1
Degree of saturation	S_r	%	68.3	10.9
Consolidated undrained triaxial tests				
Cohesion intercept	c'	kPa	5	—
Friction angle	ϕ'	°	26	—
Young's modulus at 0.1% strain	E_s	MPa	34.9	—
Young's modulus at 1% strain	E_s	MPa	10.8	—

Fig. 5. (*a*) Soil water characteristic curve (primary drying) and (*b*) shrinkage curve of site material. [Colour online]

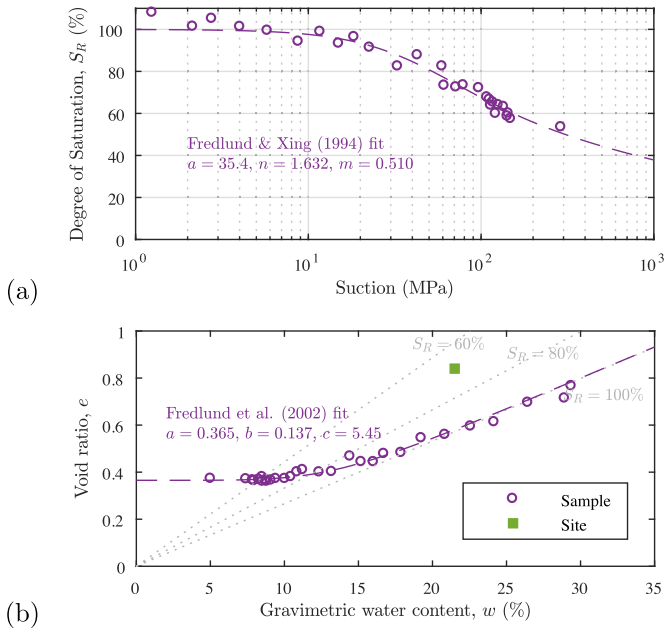

that the in situ material is in the region where large changes in volume are likely to occur as the moisture content changes. From the SWRC, the in situ estimation of the degree of saturation of 68.3% shows that this is near the point of inflection of the curve showing high potential for changes in suction as the moisture content changes. The suctions measured on site were far lower than expected from the laboratory measured SWRC; this is expected to be due to the soil in the field not being on the primary drying curve, and additional influences from the drilling resulting in lower estimates of true suction in the profile.

The 28-day and long-term strength and stiffness properties of concrete samples cast from the same batch of concrete as used in the piles are shown in Table 3. These reference samples were cured in water at 22 °C up to the day of testing. The concrete in the piles experienced approximately the same temperature for the first 28 days, after which limited strength gain would take place (as is noted in the similar strength and stiffness short and long-term results in Table 3). It was assumed that the clay surrounding the concrete below ground level would prevent the concrete from drying out, at least for the first 28 days, which would allow for strength gain similar to that of the water cured test specimen. The concrete surfaces at ground level were covered with plastic sheets to prevent drying out. It would thus be expected that the strength and stiffness of the reference concrete specimens would give a good indication of the in situ pile strength and stiffness.

Continuous surface wave (CSW) tests were conducted to determine the small-strain stiffness, G_0, of the in situ soil profile; CSW tests are described in further detail by Matthews et al. (1996) and an overview of the test procedure and com-

Table 3. Strength and stiffness properties of concrete.

Property	Symbol	Unit	28 days	7.5 months
Compressive strength	σ_c	MPa	31.4	34.9
Tensile strength	σ_t	MPa	2.0	2.0
Stiffness	E_p	GPa	26.5	27.8

Fig. 6. Small-strain stiffness results from CSW tests. Note: due to the large difference in the magnitude of the stiffness in the upper and lower layers, the same result has been plotted on two different horizontal axes so that the variation in the upper layers can still be distinguished. [Colour online]

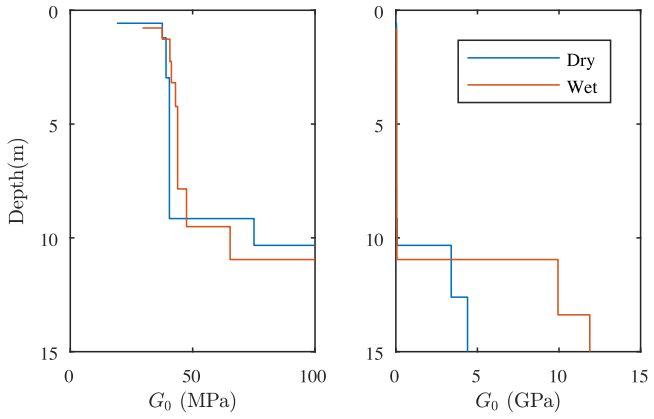

parison to other surface wave testing is given by Stokoe et al. (2004). The test provides a shear wave velocity profile from processing of the ground surface measurements induced by a vibrating energy source; elastic theory is then used to derive the stiffness profile. CSW tests provide the mass stiffness of a ground profile. These tests were conducted on the wet and dry test areas in December, i.e., two months after the wet area had been kept flooded for six months. The results are shown in Fig. 6; the average result up to 10 m depth was 37 and 41 MPa on the wet and dry sites respectively. It is interesting to note the similarity in the small-strain stiffness results on the two sites; it is expected that the intact stiffness of the wet and dry clay will be different, but due to the fissuring the small strain stiffness of the soil mass will be similar. It is the mass stiffness of the soil profile that influences the soil–pile interaction.

Cone penetration tests (CPTs) were conducted to determine the in situ undrained shear strength, c_u, of the soil; these were conducted on the wet and dry test areas eight months after the active flooding of the wet area was stopped. The CPT results are shown in Fig. 7. The water table in the wet test area was encountered at 4 m below ground level; this is a perched water table introduced by the prior flooding, and not naturally occurring. No water table was encountered in the dry test area. The classification of the soil behaviour type using the cone resistance and friction ratio according to Robertson (2010) criteria was predominantly clay and silty clay for the full depth of both profiles. The undrained shear strength was estimated using the procedure recommended by Robertson (2009); these results are also shown in Fig. 7. A layer of very dense/stiff soil was encountered between 13 and 14 m in the dry profile, and below 14.25 m in the wet profile; the shear strength results are therefore only shown to a depth of 14 m. The shear strength results show a large degree of similarity, except in the region in the wet profile which had been previously flooded and allowed to dry out, i.e., above 4 m. The portion of the profile that remained saturated had a similar strength profile to the dry site. This indicates that the dry profile can be used to get an indication of the undrained shear strength of the soil to be used in further analysis.

4. Results

The monitoring data obtained from site from the start of the flooding for a period of eleven months is reported in this section; recordings of all instrument data were taken at 15-minute intervals. The ambient weather data, results from periodic surveys, and the VWSG data are discussed, together with the processing of the VWSG data to obtain the shaft friction and axial load in the piles.

Figure 8 presents the recorded daily rainfall and minimum and maximum daily temperature data together with the dates of key events on site. The soil surface movement was measured by periodically surveying the position of installed monitoring pegs. The initial position of the pegs and benchmarks on site was measured using GPS survey relative to the nearest trig beacon. Thereafter, all levels were measured using 2 independent readings from 2 positions (4 readings) relative to a stable benchmark, and the average of these was used as the final level. Sub millimetre readings were able to be measured for each monitored point. The measurement intervals varied depending on when access was able to be gained to site and lockdown restrictions; these are shown on Fig. 8. The measured movement of the soil surface monitoring points closest to the installed piles determined from surveys of the site is shown in Fig. 9; the difference between the two readings appears larger in the dry site, although this is only due to the magnified scale in this figure. It is evident that very little movement was observed on the dry site, while substantial heave was observed on the wet site. After the initial drying out and reduction in the surface swell up until June, the soil surface movements in the dry test area are largely stable over the dry period from June to September. At the end of the test period there was an average of 59 mm of swell around the wet pile; the change in rate of swell when the surface was allowed to dry out is immediately evident. Using the Van der Merwe (1964) heave prediction method, the expected surface heave for the soil profile in the wet site is 160 mm (excluding the top 0.5 m of the profile). Despite the expected worst-case scenario

Fig. 7. Estimated undrained shear strength from CPT results. [Colour online]

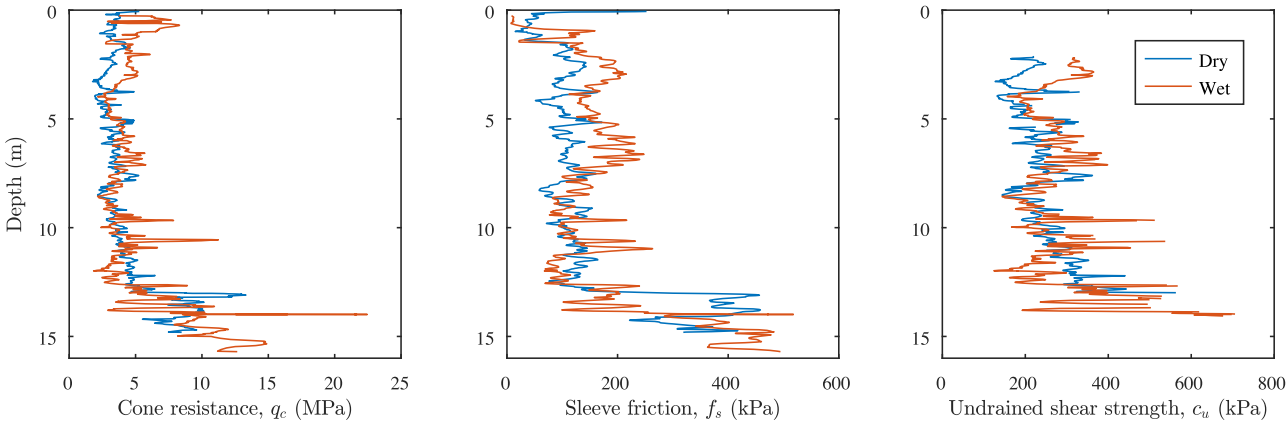

Fig. 8. Ambient weather data (daily rainfall and minimum & maximum temperatures) and key site events. [Colour online]

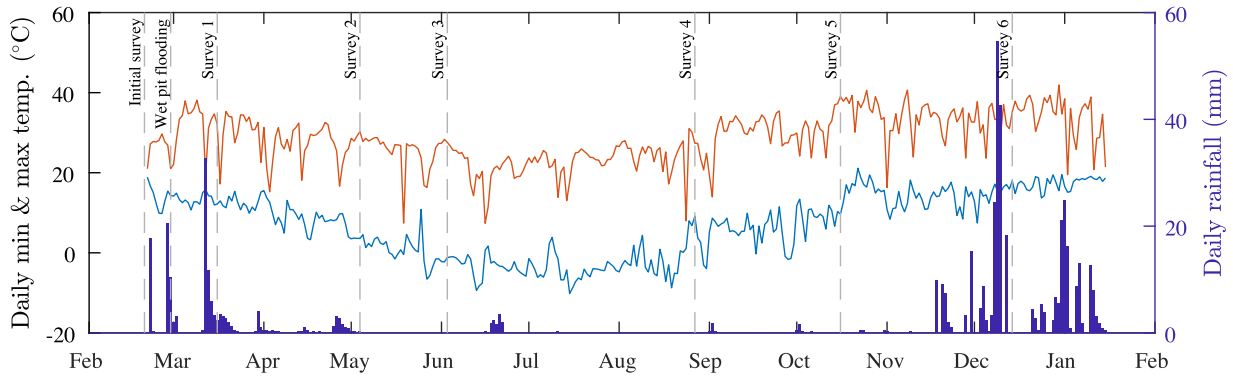

Fig. 9. Soil surface movement of monitoring points closest to the tension pile is the dry (top) and wet (bottom) areas, and average movement used in further analysis. [Colour online]

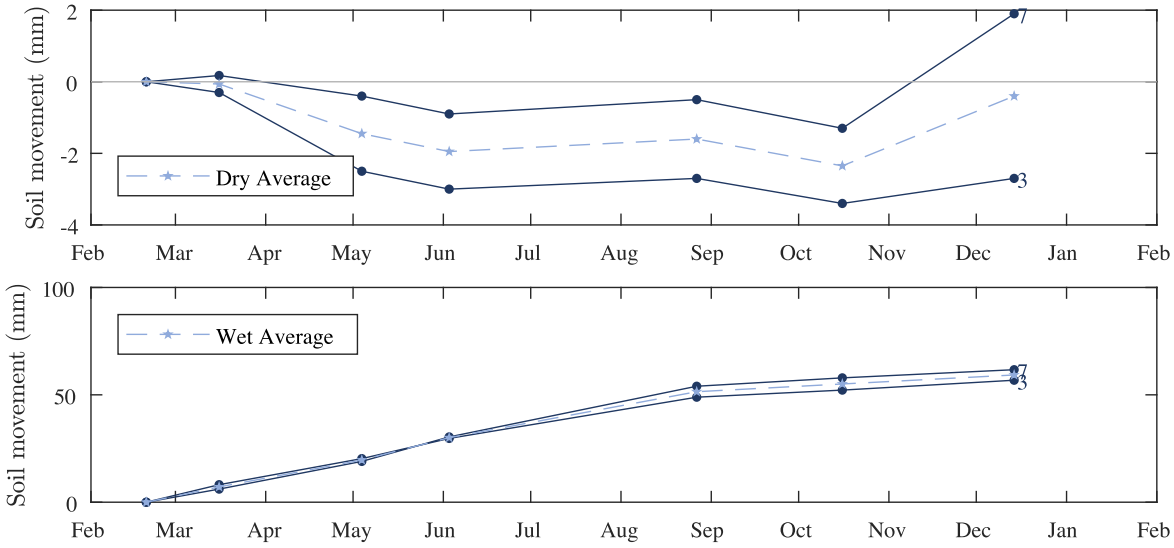

of continued flooding of the soil surface, this expected heave was not achieved. The lower measured swell on site could be due to the swell not reaching its maximum value during the study period, limited moisture ingress in the soil profile or potentially an overestimation of the Van der Merwe method.

The frequency readings of the VWSGs were converted to strain using the following relationship:

$$\Delta\mu\varepsilon = \left(\frac{F^2}{1000} - \frac{F_0^2}{1000}\right) G_F B_F \quad (5)$$

where $\Delta\mu\varepsilon$ is the change in microstrain from the initial reading, F is the frequency reading in Hz, F_0 is the initial frequency reading, and G_F and B_F are the gauge and batch factors, respectively (3.718 and 0.958 for the installed VWSGs). Due to the depth of the gauges below ground level, thermal compensation had a marginal effect on the results; the results are therefore presented without any thermal compensation. Positive axial strain is indicative of induced axial tension, and negative strain is compression.

The axial strains, ε_a, and bending strains, ε_b, in the pile were calculated according to eq. 6. The axial strains were converted to axial stress using the long-term stiffness modulus of the concrete (Table 3), and then to axial load by assuming a uniform circular cross-section of the pile. The shaft friction was calculated by dividing the difference in the pile axial load at the strain gauge locations by the surface area of the pile between the gauge depths. The assumption of a uniform cross-section was deemed to be appropriate after inspection of the bored holes before the pile was cast which showed smooth, vertical sidewalls. The core drilling showed high percentages of core recovery in the initial site investigation giving confidence in stable sidewalls throughout the depth of the profile. Slight overdrilling was noted at the base of the wet pit at the transition to the soft rock; this was below the level of the lowest VWSG pair, and would thus not impact the axial load and shaft friction calculations.

$$\varepsilon_a = \left(\varepsilon_{left} + \varepsilon_{right}\right)/2 \qquad \varepsilon_b = \left(\varepsilon_{left} - \varepsilon_{right}\right)/2 \tag{6}$$

The results of the axial and bending strain in the dry pile over the investigation period are shown in Fig. 10. The left VWSG at 3 m depth lost data from mid-July to the end of October; the recovered readings from November onwards matched the trends expected from prior to the loss and was in accordance with the expected behaviour from the other gauges. A linear interpolation was used to estimate the missing readings; this result is shown in a dashed line in Fig. 10. With the exception of the gauges at 3 m, the induced bending strains were within $\pm 10 \sim \mu\varepsilon$. The higher bending at 3 m depth is observed near the transition from the expansive to non-expansive soil profile and is expected to be as a result of uneven shrinkage around the pile, and not an anomaly of the gauge readings. Assuming uniform movement of the soil around a uniform pile, there should be no bending induced in the pile. To remove these bending effects, half the recorded bending strain was added to the recorded axial strain to calculate an effective axial strain; this only resulted in a significant difference at 3 m depth, and the result is shown in a dotted line in Fig. 10. It is evident in these results that changes in ambient temperature had as much impact on the shrinkage and swell of the soil surface as the rainfall; this explains why the construction of foundations has a marked impact on swelling of active clays, as the transpiration surface which contributes to shrinkage in the clay during the dry season is lost.

Comparing the induced strains (and thus tension/compression) with the weather and soil movement (Figs. 8 and 9), the pile initially starts to go into slight tension which corresponds to a period of high rainfall and some swell observed around the pile. The pile then starts to go into compression as the soil surface settlement increases, with a relatively stable period with minimal rainfall, temperature changes and strain changes from June to September. As the temperature starts to increase with no significant increase in rainfall (September to mid-October), there is a marked soil settlement and corresponding increase in pile compression, especially evident at 5 and 7 m depths. After the heavy December rainfall, the soil surface begins to swell again, and the recorded compression in the pile stabilises and then decreases accordingly.

The axial load and shaft friction as a function of depth is shown in Fig. 11; the boundary conditions of zero axial force at the top and base of the pile have been included, as well as the friction derived from this. As the pile goes into greater compression, the shaft friction transition from negative to positive coincides approximately with where the expansive soil transitions to non-expansive soil (4 m; Fig. 4). This confirms that the soil settlement that is inducing the compression is as a result of the shrinking of the expansive clay layer.

The axial and bending strain results of the wet pile are shown in Fig. 12. The left VWSG at 1 m depth showed unreliable results; due to the bending evident in the pile, using only a single VWSG reading to infer the axial strain was not possible. This level was thus excluded from the analysis. The two gauges at 7 m depth showed a sudden disturbance in early-May; a similar disturbance was noted at 3 m depth in mid-June and at 5 m depth in early July (evident in ε_b only).

Further inspection showed that these jumps at 7 and 5 m occurred once one of the strain gauges reached a tensile strain of $77 \sim \mu\varepsilon$; using the results from Table 3, the maximum tensile strain that the concrete can withstand is between 72 and 75 $\mu\varepsilon$. These jumps are therefore likely to be the result of the tensile capacity of the concrete being exceeded. At 7 m depth both the left and right gauges exceeded this limit, and it was assumed that the tensile stress in the pile was carried by the reinforcing bars after this point; the change in slope of the strain readings indicates this change. At 3 m depth, the jumps occurred in both gauges at a recorded average tensile strain of 55 $\mu\varepsilon$; the overall tensile capacity of the pile is not exceeded, however, it is possible that this is the result of the formation of a local crack around the gauge. The modified measurements without the jumps are shown in dashed lines in Fig. 12.

Figure 12 shows a clear trend of bending in the pile in one direction up until the crack at the transition, presumably introduced by uneven swell around the pile. Thereafter minimal bending at the crack depth is noted; however, continued bending above and below this level is noted. The adjusted axial strain removing the effects of bending is presented in Fig. 13; this is more consistent with the expected behaviour as the full length of the pile remains in tension which corresponds to continued surface swell over this period. The tensile strain limit of the concrete is plotted in this figure; once the effective axial strain measured by the VWSGs exceeded this limit, the tensile stress and axial load in the pile was calculated using the steel stiffness ($E_s t = 200$ GPa) and area properties.

Fig. 10. Measured axial and bending strain in the dry pile (interpolated data shown in dashed line; adjusted ε_a to account for bending shown in dotted line in the top figure). [Colour online]

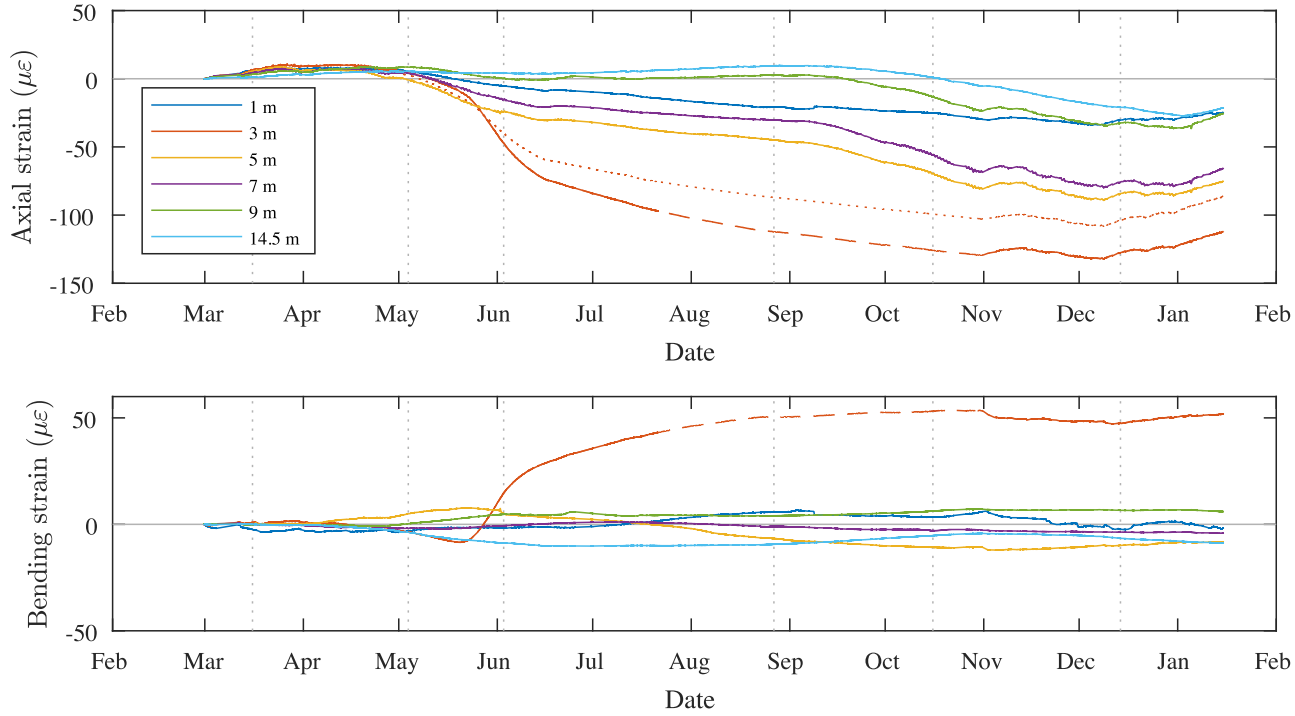

Fig. 11. Axial load and shaft friction as a function of depth in the dry pile (data derived from the adjusted axial strain is plotted by the stars, with connected points shown in dashed lines). [Colour online]

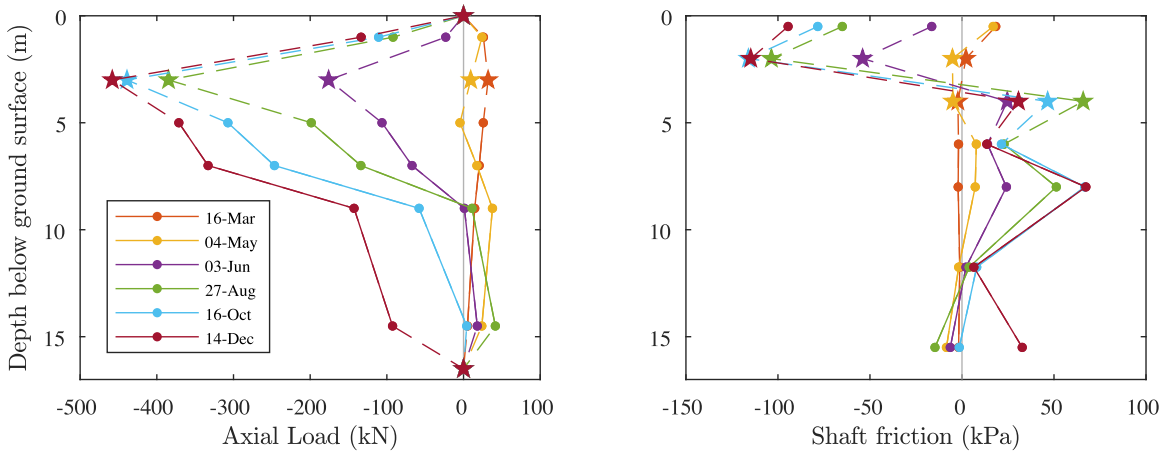

The axial load and shaft friction as a function of depth is shown in Fig. 14; the change from positive to negative shaft friction occurs at 5.5 m for the first measurement, but then stabilises between 6.8 and 7.2 m depth for the subsequent measurements which corresponds to the expected depth of the expansive clay at this location (Fig. 3). The increase in swell up until September was linear; however, the maximum axial load shows a tendency towards a limiting value, with large initial increases in tension and limited increases in the maximum load, and more of a "load-sharing" effect with a broadening of the peak load.

5. Discussion and analysis

The benefit of being able to accurately predict the uplift force on piles in expansive clays is twofold: first, to design the appropriate required structural capacity of the pile, especially for lightly loaded structures where the pile would be loaded in tension, and second, to allow an estimate of pile head movement and design the required length of pile in the stable soil zone to resist the upward movement with an adequate factor of safety. This is analogous to the approach to design piles in settling soil with negative skin friction and corresponding drag forces and settlement as discussed by Poulos (2008).

Fig. 12. Measured axial and bending strain in the wet pile (modified data shown in dashed lines). [Colour online]

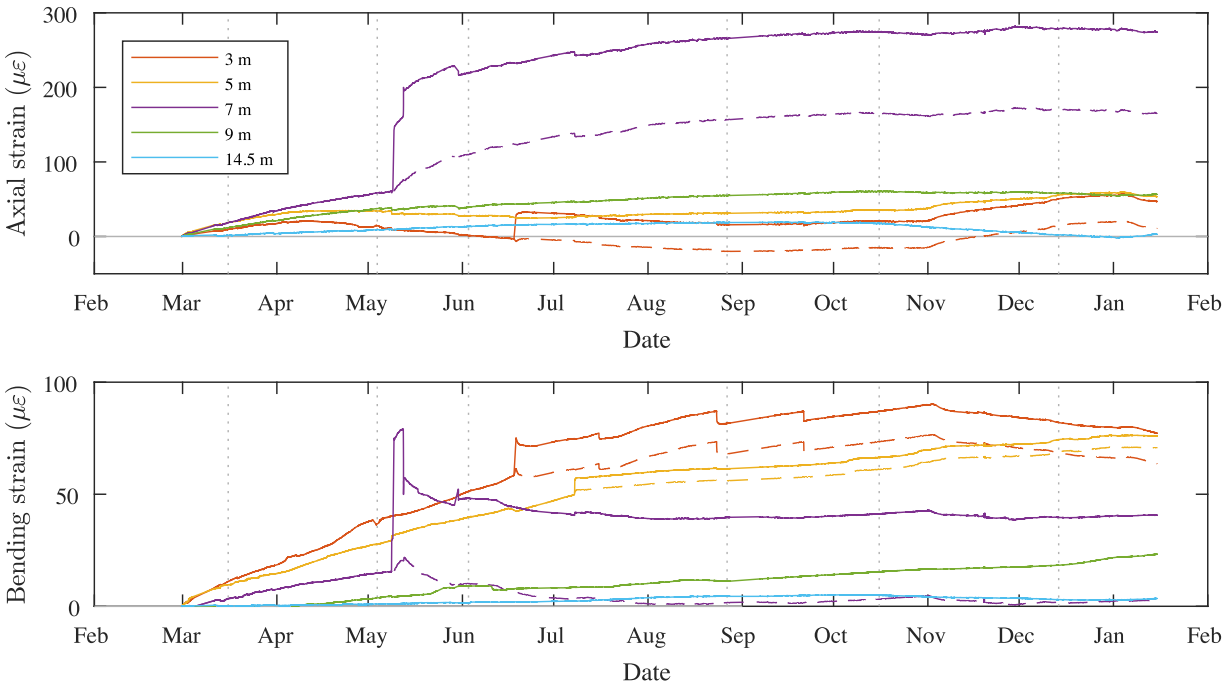

Fig. 13. Corrected axial strain in the wet pile to remove the effects of bending (results derived from previously extrapolated data shown in dash-dot line). [Colour online]

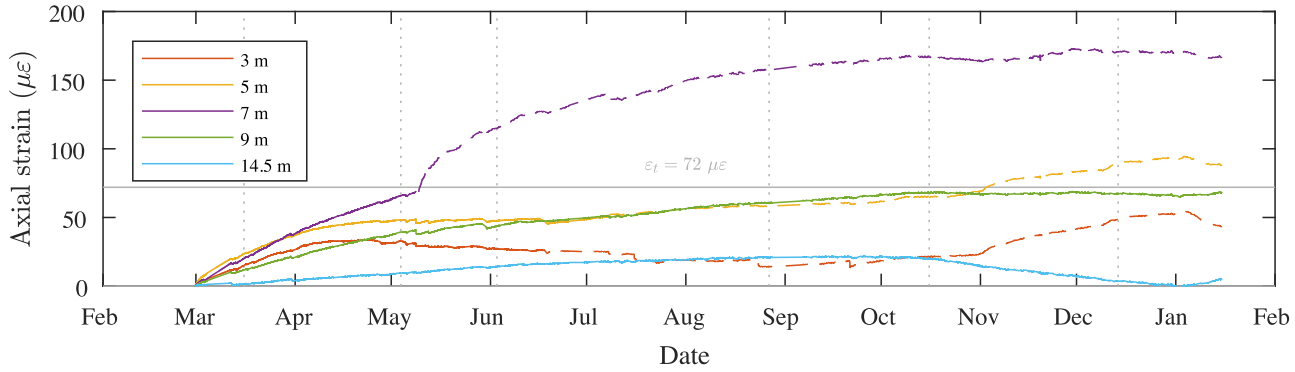

The results for the measured tension in the wet pile were compared to the various prediction methods discussed in Section 2 as a validation to determine the applicability of the presented methods. The soil properties used for the analysis are shown in Table 4. The peak undrained shear strength was estimated from the average value of the CPT estimate in the upper 7 m of the dry profile. An additional estimate of the undrained shear strength was made using the remoulded shear strength which is equal to the measured sleeve friction, f_s, in the CPT profile. Given the large movements in the soil due to swell, the shear modulus of the soil was calculated at large strains using a relationship of $G_s/G_0 = 0.15$ at 1% shear strain (Clayton and Heymann 2001); the resulting soil modulus (E_s) matches the recommended value from Poulos and Davis (1980) for bored piles based on the soil c_u and matches well with the laboratory measurements in Table 1. The field measurements of stiffness were used in the analysis as these are expected to have a better match to the bulk behaviour of the soil.

The predicted axial load and shaft friction in the expansive layer of the soil from the total and effective stress methods is shown in Fig. 15*a* using both the peak and remoulded estimates of the undrained shear strength. These methods assume that the neutral plane occurs at the transition from the swelling to the stable soil, and that the shaft friction above this plane is fully mobilised. Only a single prediction is possible with these methods, and a prediction of the tensile load as a function of the soil heave is not possible. The shape of the increase in load and friction with depth for the effective stress method did not show a good match to the measured behaviour in Fig. 14. In contrast, the assumption of a constant shaft friction from the total stress method shows a reasonable comparison, particularly as the soil started to swell. The use of the remoulded undrained shear strength shows a bet-

Fig. 14. Axial load and shaft friction as a function of depth in the wet pile, plotted using effective axial strain from Fig. 13 (modified data are plotted by the stars, with connected points shown in dashed lines; axial load in the grey block calculated using steel properties). [Colour online]

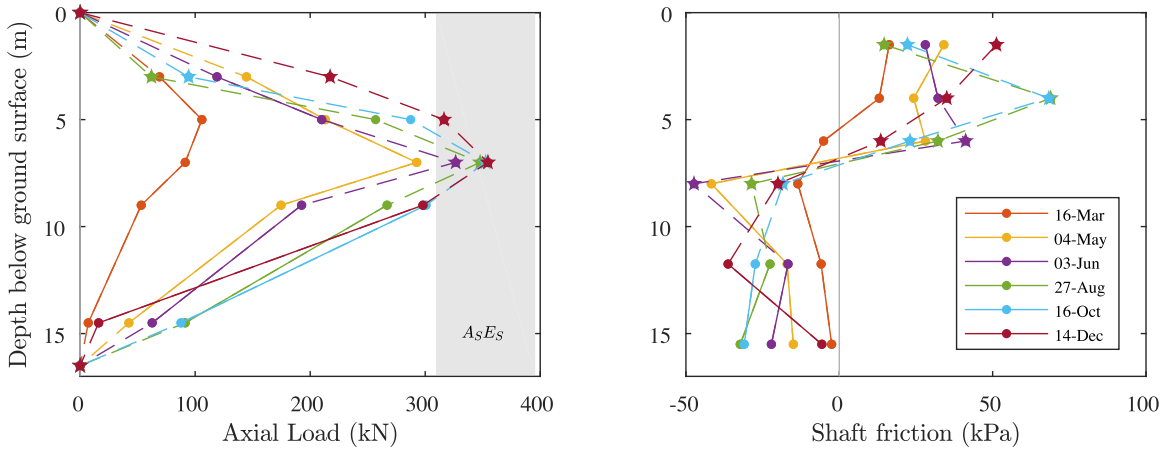

Table 4. Soil properties used in analysis.

Soil property	Symbol	Unit	Value	Reference
Cohesion intercept	c'	kPa	5	Table 2
Effective friction angle	ϕ'	°	26	Table 2
Unit weight	γ	kN/m^3	17	Table 2
Peak undrained shear strength	c_u	kPa	206	Fig. 7
Remoulded undrained shear strength	f_s	kPa	91	Fig. 7
Poisson Ratio	ν	—	0.3	Assumed
Small strain shear modulus	G_s	MPa	39	Fig. 6
Shear modulus of soil	G_s	MPa	5.85	$G_s/G_0 = 0.15$ at 1% shear strain*
Elastic modulus of soil	E_s	MPa	15.2	$E_s = 2G_s(1+\nu)$

*Clayton and Heymann (2001).

ter match to the measured shaft frictions and peak axial load than the peak undrained shear strength.

The predicted load and friction using the measured soil surface movements and the elastic solution presented in eq. 4 are shown in Fig. 15*b* for three selected dates of 16 March, 4 May and 14 December using an active depth of $H = 7$~m. The average soil surface swell on these dates were 7, 30, and 59 mm, respectively (Fig. 9). These results are based on an assumed linear swell profile from zero at the transition from expansive to swelling clay, to the measured value at the surface (see Fig. 1), and additionally assume that there is no pile–soil slip that occurs. The result in Fig. 15*b* was found to be highly sensitive to the shear modulus of the soil G_s. It is apparent that as the soil heave increases, this method significantly overestimates the tension developed in the pile; the maximum measured tension was 355 kN, whereas a maximum tension of 934 kN is predicted at the date of the latest survey. The required shaft friction needed to develop this load far exceeds that which was measured (compare the shaft friction in Fig. 15*b* to that in Fig. 14). It could therefore be argued that due to the large amount of swell, there is slip occurring between the soil and the pile, and a limiting value of shaft friction needs to be applied. A second observation from the shaft friction predicted by the elastic analysis is that with an active depth of 7 m, the transition, i.e. neutral plane, does not occur at the boundary of the expansive clay and residual soil, but rather within the clay profile. Detailed inspection of the result shows that this transition occurs at a depth of 5.5 m.

To incorporate the effect of relative slip between the pile and the soil, the elastic results were modified to apply a limiting maximum shaft friction in the expansive clay. This is the same modification made by Poulos and Davis (1980) to account for soil slip. To do this, the elastic solution as presented in eq. 4 was used to calculate the required shaft friction as shown in Fig. 15; where the required shaft friction exceeded the chosen limiting value, the shaft friction was set to the limiting value. The required resistance in the stable soil zone to ensure that the boundary condition of zero load at the pile toe is met was then iteratively calculated.

An estimate of the limiting shaft friction can be made using the αc_u-value, or αf_s-value; this gives 92.7 kPa and 40.95 kPa, respectively. An alternative method making direct use of CPT data is recommended by Eslami and Fellenius (1997) using the effective cone resistance, $q_E (= q_c - u)$, multiplied by the shaft correlation coefficient, C_S. The expansive clay layer classified in both the Silty clay – Stiff clay (Zone 3)

Fig. 15. Predicted axial load and shaft friction due to swelling (*a*) using total and effective stress methods and (*b*) using elastic solution. [Note: the axes in (*a*) and (*b*) are scaled differently for better reading of the results.] [Colour online]

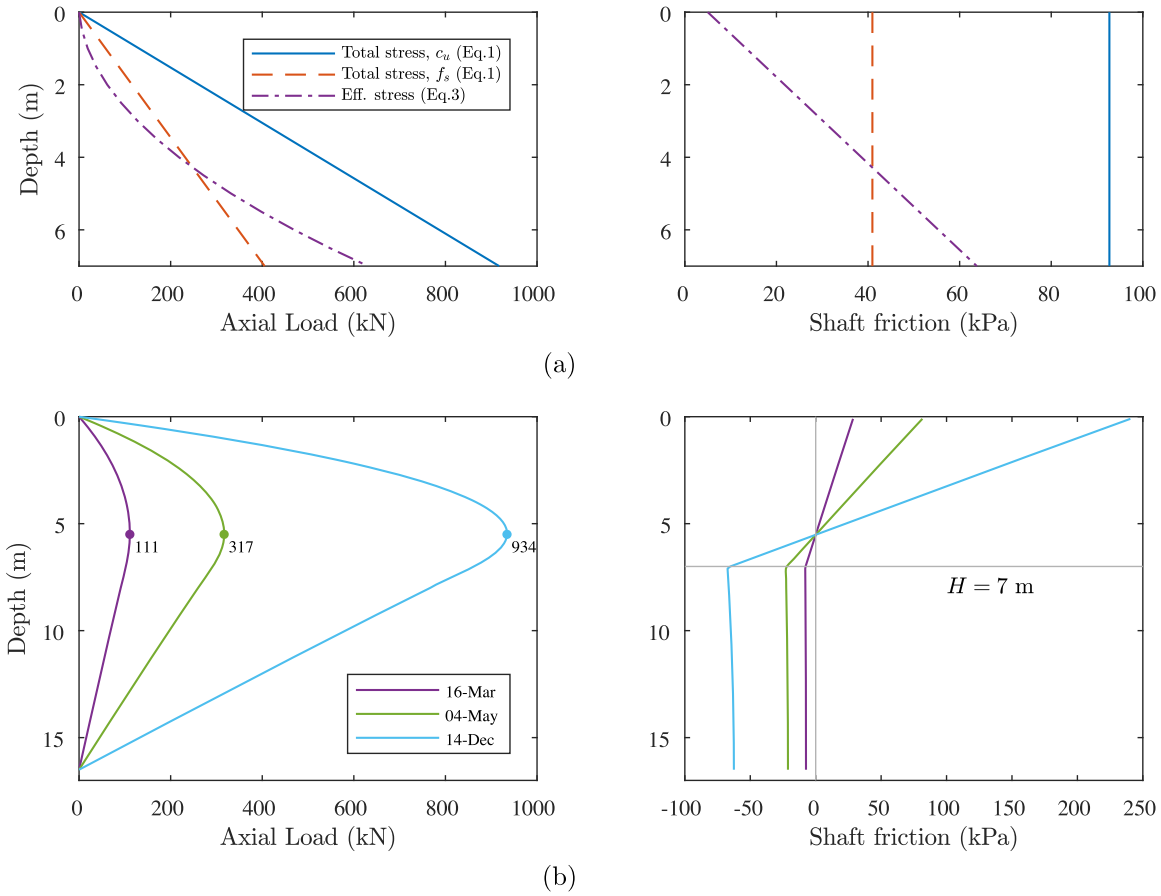

and Silty sand – Sandy Silt (Zone 4) in the Eslami and Fellenius (1997) profiling chart. The recommended value of C_S for these materials is 2.5% and 1%, respectively. Using an average of the two values, the limiting shaft friction is estimated as 56.2 kPa. The maximum shaft friction in the final measurement in Fig. 14 is approximately 50 kPa; the estimated value of limiting shaft friction of 56.2 kPa was therefore used in further analysis. The required constant friction in the resistance portion of the pile needed to ensure the boundary condition of zero load at the pile tip was then calculated.

The results of the predicted axial load with the inclusion of a limiting shaft friction using the elastic method are shown in Fig. 16 in comparison to the measured site data. The results of the original elastic results from Fig. 15*b* are also included for ease of comparison. The larger the length of exceeded shaft friction (see Fig. 15*b*), the greater the difference made by the revised solution. For the first date shown, the revised result is equivalent to the original result as the limiting shaft friction was not exceeded. The figure shows that for the first prediction (16-Mar), the elastic method shows an excellent match to the measured data both in terms of magnitude and shape of the profile; the predicted and measured friction transition also match excellently. For the later predictions, the magnitude of the elastic predictions match the magnitude of the

Fig. 16. Predicted axial load on wet pile using modified elastic solution in comparison to measured results and original elastic solution. [Colour online]

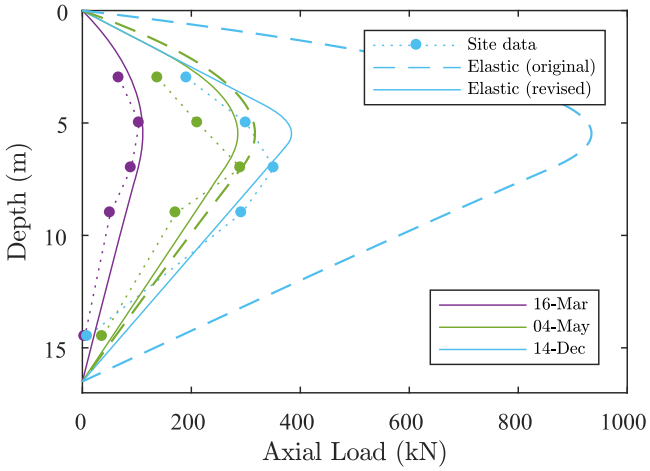

measured axial loads well (within 10% for the final measurement made), although the measured data shows the location of the neutral plane occurring deeper in the soil than what is predicted by the elastic method. This potentially indicates

that there is a slightly thicker expansive clay than was originally anticipated, and that over time, as the water had more time to infiltrate deeper in the soil, the deeper expansive clay also started to expand and contributed to the uplift force generated in the pile.

Considering the behaviour of the dry pile (Fig. 11), it is interesting to note that despite significantly lower movement in the soil around this pile compared to the pile in the flooded area and also the presumed thinner layer of expansive material compared to the wet pile location, the induced axial force (maximum compression of 450 kN, Fig. 11) is greater than that of the wet pile (maximum tension of 355 kN, Fig. 14). The axial load in the pile from theoretical estimates would be the same as shown for the total stress (eq. 1) and effective stress (eq. 3) in Fig. 15*a*, with an induced axial compression instead of tension. There may be a slight difference due the bulging of the pile in compression resulting in increased shaft friction; this is expected to be nominal. The observed shaft friction around the upper portion of the dry pile is approximately 125 kPa. To achieve a shaft friction this high, the total stress method would need to be applied using the peak undrained shear strength with an α-value of 0.6. This large induced shaft friction and corresponding compression is interesting especially for the potential that this could add to the required capacity of piles installed in expansive clays where shrinkage as well as heave could reasonably be expected. Longer-term monitoring of this pile is planned to observe how the axial load changes over several seasons of natural moisture content changes in the soil and resultant soil movement.

6. Conclusion

A large-scale field trial was conducted to measure the axial loads in a bored concrete pile installed in a highly expansive clay and socketed in a stable layer beneath the active zone. Swelling of the soil was accelerated by flooding the soil surface. The results showed a large initial increase in the induced tension, with smaller increases over time, even though the soil swell largely continued at the same rate. The reduction in the increased tension over time was expected to be due to larger soil movements exceeding the available shaft friction which tended to a constant value with depth in the swelling clay. Cracking of the pile was deemed to occur at the base of the top of the active clay layer. The assumption of a uniform strength profile consistent with total stress methods showed a better match to the inferred shaft friction from the strain measurements in the pile than an increasing strength profile from effective stress methods. The total stress methods provide a conservative estimate of the expected uplift force assuming that the neutral plane occurs at the transition from the expansive to stable soil; the use of the remoulded undrained shear strength provided a closer match to the measured load than the peak undrained shear strength. The elastic prediction method for induced tension, modified to allow for a maximum mobilised shaft friction and thus incorporate pile–soil slip, showed an excellent match to the measured results, and allows for predictions of tension as a function of soil heave.

List of symbols

A_p	cross-sectional area of the pile
A_s	cross-sectional area of the steel in the pile
c_u	undrained shear strength of soil
c'	effective cohesion of soil
$C_{1,2,3,4}$	coefficients for elastic pile force solution
C_S	shaft correlation coefficient
D	pile diameter
e	void ratio
E_p	modulus of elasticity of the pile
E_s	modulus of elasticity of the soil
E_st	modulus of elasticity of the steel
f	shaft friction
f_s	measured sleeve friction in CPT
F	frequency reading from VWSG
F_u	uplift force acting on pile
G_0	small strain stiffness of soil
G_s	shear modulus of the soil
h	depth of soil from the surface
H	thickness of active soil layer
K	coefficient of lateral stress
L	length of pile
P	axial load on pile
PI	plasticity Index
P_S	vertical swell pressure
q_c	cone resistance (CPT)
q_E	effective cone resistance (CPT), $q_c - u$
r_m	maximum effective radius around the pile
r_0	pile radius
s_0	heave at the soil surface
S_r	degree of saturation
u	measured pore pressure (CPT)
z	depth of soil from the surface
α	shaft adhesion factor
α	simplification factor (eq. 4), $\alpha^2 = 2\pi/\lambda_p A_p \zeta$
σ'_h	horizontal effective stress
σ'_v	vertical effective stress
σ_c	compressive strength of concrete
σ_t	tensile strength of concrete
ϕ'	effective internal angle of friction
γ	unit weight of soil (kN/m^3)
ν	poisson ratio of soil
λ_p	pile to soil stiffness ratio, $\lambda_p = E_p/G_s$
ζ	effective parameter of the pile radius, $\zeta = \ln(r_m/r_0)$

Acknowledgements

The authors gratefully acknowledge the financial support from the UK Engineering and Physical Sciences Research Council (EPSRC) Global Challenges Fund under the Wind Africa project, Grant Ref: EP/P029434/1. The following people are acknowledged for assistance and support in the field installation: Neale Baardjies and Bethuel Mphasa from Yellowstar Mining; Sarel Coetzer, Rikus Kock (in memoriam), and Dr. Gerrit Smit from the University of Pretoria; and Dr. Khalid Abdalla and Dr. Nicky de Battista from the University of Cambridge. Prof. Gerhard Heymann from the University of

Pretoria is thanked for the provision of the CSW test results. Lucy Eost and Dr. Tiago Gaspar from Durham University are thanked for the provision of the SWRC and shrinkage test results.

Article information

History dates

Received: 17 February 2021
Accepted: 31 May 2022
Accepted manuscript online: 10 June 2022
Version of record online: 4 November 2022

Copyright

Data availability

Some or all data used are available from the corresponding author by request.

Author information

Author ORCIDs

T.S. da Silva Burke https://orcid.org/0000-0001-9393-8601
S.W. Jacobsz https://orcid.org/0000-0002-7439-2276
M.Z.E.B. Elshafie https://orcid.org/0000-0001-9908-5515
A.S. Osman https://orcid.org/0000-0002-5119-8841

Author notes

Formerly, T.S. da Silva Burke was a Research Associate at the University of Cambridge, Cambridge, United Kingdom.

Author contributions

TB: project administration, investigation, formal analysis, writing—original draft, writing—review and editing; SJ: funding acquisition, conceptualization, project administration, formal analysis, writing—review and editing; ME: funding acquisition, conceptualization, supervision, writing—review and editing; AO: funding acquisition, conceptualization, writing—review and editing.

Competing interests

The authors declare that there are no competing interests.

Supplementary material

Supplementary data are available with the article at https://doi.org/10.1139/cgj-2021-079.

References

ASTM D422-63e2 2007. Standard Test Method for Particle-Size Analysis of Soils. American Society for Testing and Materials (ASTM) International, West Conshohocken, Pennsylvania.

Blight, G. E. 1984. Power station foundations in deep expansive soil. *In* International Conference on Case Histories in Geotechnical Engineering. University of Missouri–Rolla.

Burland, J. 1973. Shaft friction of piles in clay–a simple fundamental approach. Ground Engineering, **6**(3): 30–42.

Byrne, G., Chang, N., and Raju, V. 2019. A guide to practical geotechnical engineering in Africa. 5th ed., Franki A Keller Company.

Challa, P.K., and Poulos, H.G. 1991. Behaviour of single pile in expansive clay. Geotechnical Engineering, **22**: 189–216.

Chandler, R.J. 1968. The shaft friction of piles in cohesive soils in terms of effective stress. Civil Engineering and Public Works Review, **60**: 48–51.

Clayton, C. R.I., and Heymann, G. 2001. Stiffness of geomaterials at very small strains. Géotechnique, **51**: 245–255. doi:10.1680/geot.2001.51.3.245.

Collins, L.E. 1953. A preliminary theory for the design of underreamed piles. The South African Institution of Civil Engineers, **3**.

Elsharief, A.M., Ahmed, E.O., and Mohamedzein, Y.E.-A. 2016. Guidelines for the design of bored concrete piles in expansive soils of Sudan. Journal of Building and Road Research, **8**.

Eslami, A., and Fellenius, B.H. 1997. Pile capacity by direct CPT and CPTu methods applied to 102 case histories. Canadian Geotechnical Journal, **34**: 886–904. doi:10.1139/t97-056.

Fan, Z.-h., Wang, Y.-h., Xiao, H.-b., and Zhang, C.-s. 2007. Analytical method of load-transfer of single pile under expansive soil swelling. Journal of Central South University of Technology, **14**: 575–579. doi:10.1007/s11771-007-0110-4.

Fredlund, D.G., and Xing, A. 1994. Equations for the soil-water characteristic curve. Canadian Geotechnical Journal, **31**: 521–532. doi:10.1139/t94-061.

Fredlund, M.D., Wilson, G.W., and Fredlund, D.G. 2002. Representation and estimation of the shrinkage curve. In: Proc., 3rd Int. Conf. on Unsaturated Soils, UNSAT 2002. pp. 145–149.

Jennings, J.E. 1962. The heaving of buildings and the associated economic consequences, with particular reference to the Orange Free State goldfields. Civil Engineering, **1962**: 221–248.

Jiang, J., Hou, K., and Ou, X. 2020. Analysis of the bearing capacity of a single pile based on an analytical solution of pile–soil interaction in expansive soil. Geotechnical and Geological Engineering, **38**: 1721–1732. doi:10.1007/s10706-019-01126-2.

Jones, D.E., and Holtz, W.G. 1973. Expansive soils—the hidden disaster. Civil Engineering, **43**.

Matthews, M., Hope, V., and Clayton, C. Rayleigh., 1996. The use of surface waves in the determination of ground stiffness profiles. Proceedings of the Institution of Civil Engineers-Geotechnical Engineering, **119**: 84–95. doi:10.1680/igeng.1996.28168.

Meintjes, H., and Pellissier, J. 1994. An experimental pile in deep residual expansive clay. In: International Conference on Soil Mechanics and Foundation Engineering. pp. 487–492.

Morin, W. 1971. Properties of African tropical black clay soils. In: Proceedings of the Regional Conference for Africa on Soil Mechanics and Foundation Engineering. pp. 51–59.

Poulos, H.G. 1989. Program PIES Axial Response of Piles in Expansive Soils. Centre for Geotechnical Research, University of Sydney, Sydney, NSW.

Poulos, H.G. 2008. A practical design approach for piles with negative friction. Proceedings of the Institution of Civil Engineers-Geotechnical Engineering, **161**: 19–27. doi:10.1680/geng.2008.161.1.19.

Poulos, H.G., and Davis, E.H. 1980. Pile foundation analysis and design. John Wiley & Sons.

Robertson, P.K. 2009. Interpretation of cone penetration tests—a unified approach. Canadian Geotechnical Journal, **46**: 1337–1355. doi:10.1139/T09-065.

Robertson, P.K. 2010. Soil behaviour type from CPT: an update. *In* Proceedings of the 2nd International Symposium on Cone Penetration Testing, CPT'10. Cone Penetration Testing Organizing Committee, pp. 575–583.

SANS 3001-GR1, 2013. Civil engineering test methods Part GR1: Wet preparation and particle size analysis. Standard, South African Bureau of Standards, Pretoria.

SANS 3001-GR10, 2014. Civil engineering test methods Part GR10: Determination of the one-point liquid limit, plastic limit, plasticity index and linear shrinkage. South African Bureau of Standards, Pretoria.

SANS 3001-GR3, 2014. Civil engineering test methods Part GR3: Particle size analysis of material smaller than 2 mm (hydrometer method). South African Bureau of Standards, Pretoria.

Skempton, A.W. 1959. Cast in-situ bored piles in London clay. Geotechnique, **9**: 153–173. doi:10.1680/geot.1959.9.4.153.

Stokoe, K.H., Joh, S.-H., and Woods, R.D. 2004. Some contributions of in situ geophysical measurements to solving geotechnical engineering problems. *In* Proceedings ISC-2 on Geotechnical and Geophysical Site Characterization. Millpress, pp. 97–132.

Van der Merwe, D.H. 1964. The prediction of heave from the plasticity index and percentage clay fraction of soils. The Civil Engineer in South Africa, **1964**: 103–107.

Williams, A.A.B., Pidgeon, J.T., and Day, P.W. 1985. Expansive soils: problem soils in South Africa-state of the art. The Civil Engineer in South Africa, **27**: 367–401.

Xiao, H.-b., Zhang, C.-s., Wang, Y.-h., and Fan, Z.-h. 2011. Pile–soil interaction in expansive soil foundation: analytical solution and numerical simulation. International Journal of Geomechanics, **11**: 159–166. doi:10.1061/(ASCE)GM.1943-5622.0000046.